Structural, magnetic and electronic properties of $RNiO_3$ perovskites (R = rare earth)

1997 J. Phys.: Condens. Matter 9 1679

(http://iopscience.iop.org/0953-8984/9/8/003)

J. Phys.: Condens. Matter **9** (1997) 1679–1707. Printed in the UK PII: S0953-8984(97)77266-7

REVIEW ARTICLE

Structural, magnetic and electronic properties of $RNiO_3$ perovskites (R = rare earth)

María Luisa Medarde

Laboratory for Neutron Scattering, ETH Zürich & PSI, CH-5332 Villigen PSI, Switzerland

Received 17 July 1996, in final form 14 October 1996

Abstract. $RNiO_3$ perovskites (R = rare earth) provide a remarkable opportunity to study the relationship between structural and physical properties since, by moving along the 4f rare earth series, the evolution of several transport and magnetic properties can be nicely correlated to the steric effects associated with the lanthanide contraction. The most appealing example is probably the metal–insulator transition discovered for the compounds with R $\neq$ La, whose critical temperature T_{M-I} increases with decreasing size of the rare earth ion. On the other hand, several experimental results show that in $RNiO_3$ perovskites the degree of Ni 3d–O 2p hybridization is extremely high. The purely ionic (Ni^{3+} O^{2-}) configuration, first suggested by neutron diffraction experiments, has been then substituted by a ground state where the $3d^7 2p^6$ (Ni^{3+} O^{2-}) and $3d^8\underline{L}$ (Ni^{2+} O^-) configurations are strongly mixed. In this paper, a summary of the scientific work performed on the $RNiO_3$ system during the last 6 years is presented. The results of the different experimental techniques are successively reviewed, with special emphasis on the relationship between the structural and the physical properties. The possible mechanisms responsible for the metal–insulator transition, which is the major open question for $RNiO_3$ perovskites, are also discussed.

Contents

0953-8984/97/081679+29$19.50

1. Introduction

Very few systems allow the study of the relationship between structural changes and physical properties in such a clear way as $RNiO_3$ perovskites (R = rare earth). Synthesized for the first time by Demazeau *et al* [1] in 1971 and completely forgotten for almost twenty years, these compounds have regained interest since the discovery of high-temperature superconductivity and giant magnetoresistive effects in other perovskite-related systems.

Although the nickelates do not display any of these exotic properties, they are, together with cuprates and manganites, one of the rare families of oxides which show metallic conductivity. Moreover, resistivity measurements have revealed the existence of a very sharp metal–insulator (M–I) transition in the compounds with R ≠ La [2, 3] (see figure 1(a)). The evolution of T_{M-I} along the series can be correlated with the degree of deviation of each compound from the ideal perovskite structure, which increases as La is substituted by the smaller-sized rare earth ions. Moreover, the M–I transition is accompanied by a small expansion of the unit cell volume (about 0.2%, see figure 1(b)) [4]. For the first members of the series ($PrNiO_3$ and $NdNiO_3$), a sudden appearance of 3D (three-dimensional) ordered $S = 1/2$ magnetic moments at the Ni sites has also been observed simultaneously with the electronic localization. In contrast, for the remaining rare earths, the onset of the Ni magnetic ordering takes place at a temperature T_N considerably lower than T_{M-I} (see figure 1(c) and table 1).

Table 1. Room-temperature structural data, M–I temperature and the Néel temperature for $RNiO_3$ perovskites.

	S.G.	a (Å)	b (Å)	c (Å)	t	d_{Ni-O} (Å)	θ (°)	T_{M-I} (K)	T_N (K)
$LaNiO_3$	$R\bar{3}c$	5.4573(1)[a]	5.4573(1)[a]	13.1462(3)[a]	0.9856	1.935(1)[a]	165.2(1)[a]	metallic	paramagnetic
$PrNiO_3$	*Pbnm*	5.4193(1)[a]	5.3801(1)[a]	7.6263(1)[a]	0.9751	1.942(1)[a]	158.7(1)[a]	130[b]	130[c]
$NdNiO_3$	*Pbnm*	5.3891(3)[a]	5.3816(2)[a]	7.6101(3)[a]	0.9711	1.942(1)[a]	157.1(6)[a]	200[b]	200[c]
$SmNiO_3$	*Pbnm*	5.3252(2)[d]	5.4247(2)[d]	7.5608(2)[d]	0.9642	1.949(1)[d]	153.4(1)[d]	400[b]	225[e]
$EuNiO_3$	*Pbnm*	5.293(2)[f]	5.466(2)[f]	7.542(3)[f]	0.9620	[g]	147.9[h]	420[i]	205[d,e]
$GdNiO_3$	*Pbnm*	5.258(2)[f]	5.492(2)[f]	7.506(3)[f]	0.9569	[g]	143.1[h]	[g]	180[g,j]
$DyNiO_3$	*Pbnm*	5.212(2)[f]	5.500(2)[f]	7.445(3)[f]	0.9507	[g]	139.5[h]	[g]	163[g,j]
$HoNiO_3$	*Pbnm*	5.181(2)[f]	5.510(2)[f]	7.425(3)[f]	0.9460	[g]	136.2[h]	[g]	148[g,j]
$YNiO^3$	*Pbnm*	5.178(2)[f]	5.516(2)[f]	7419(3)[f]	0.9452	[g]	135.8[h]	[g]	145[k]
$ErNiO_3$	*Pbnm*	5.160(2)[f]	5.514(2)[f]	7.381(3)[f]	0.9423	[g]	135.4[h]	[g]	144[g,j]
$TmNiO_3$	*Pbnm*	5.149(2)[f]	5.495(2)[f]	7.375(3)[f]	0.9379	[g]	135.4[h]	[g]	144[g,j]
$YbNiO_3$	*Pbnm*	5.131(2)[f]	5.496(2)[f]	7.353(3)[f]	0.9354	[g]	134.2[h]	[g]	138[g,j]
$LuNiO_3$	*Pbnm*	5.117(2)[f]	5.499(2)[f]	7.356(3)[f]	0.9318	[g]	132.5[h]	[g]	130[k]

[a] Neutron diffraction data [4].
[b] From [2].
[c] From neutron diffraction [27].
[d] Neutron diffraction data [28].
[e] From μ+SR [3].
[f] X-ray diffraction data [1].
[g] Not measured.
[h] Calculated from the cell parameters given in [1] by using the relation $\theta = \pi - 2a\cos(a^2\sqrt{2}/bc)$.
[i] From [3].
[j] Extrapolated.
[k] From susceptibility data [1].

Concerning the electronic structure, the value of the magnetic moment ($\approx 1\ \mu_B$) first suggested a ground state not too far from the purely ionic Ni $3d^7$ O $2p^6$ (Ni^{3+} O^{2-})

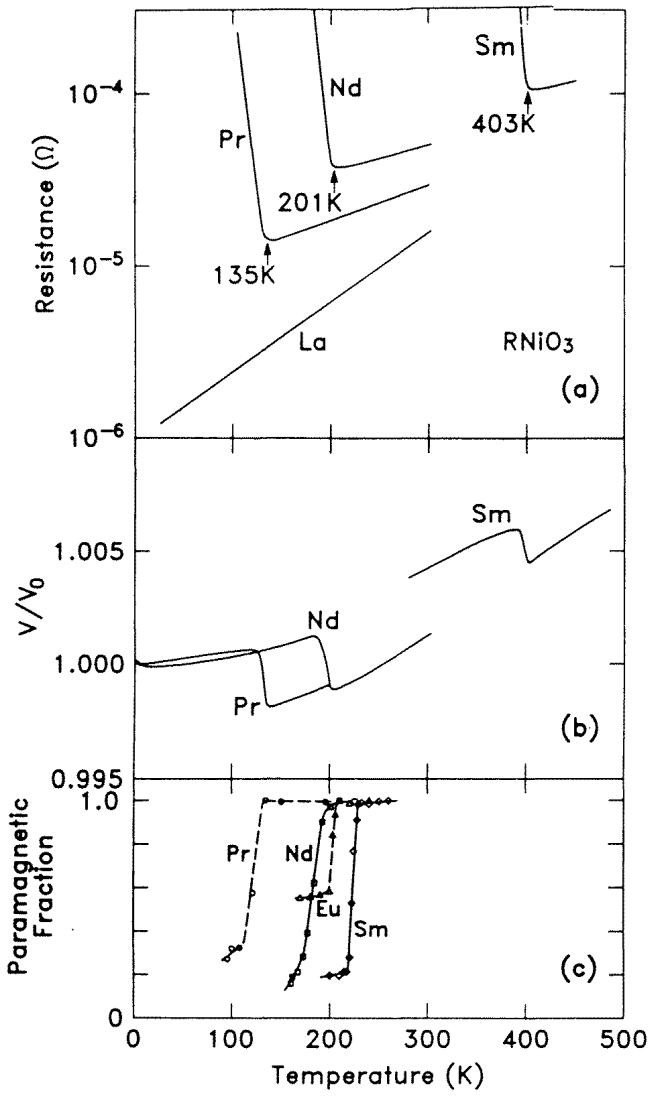

Figure 1. (a) The electrical resistance of $LaNiO_3$, $PrNiO_3$, $NdNiO_3$ and $SmNiO_3$ showing their metal–insulator transitions. (b) The temperature dependence of the relative unit cell volume showing the anomaly at T_{M-I}. (c) The paramagnetic fraction as determined from muon$^+$ spin rotation experiments, which drops suddenly at the antiferromagnetic ordering temperature (from [3], reproduced with permission of the authors).

configuration. However, recent spectroscopic measurements indicate that the degree of hybridization between the Ni 3d and O 2p orbitals is extremely high [5–7]. A description including covalency has then been proposed by several authors. The ground state is then described as $|\Psi^G_{covalent}\rangle = \alpha|3d^7 2p^6\rangle + \beta|3d^8\,\underline{L}\rangle$, the weight of the $3d^8\,\underline{L}$ configuration ranging between 30 and 70%.

In spite of some theoretical calculations [8], which suggest a charge-transfer nature for the gap, the mechanism responsible for the M–I transition is controversial at the present time [5]. Several origins can be considered, but the main difficulty, especially for the Pr and Nd compounds, is to establish the hierarchy between the three kind of effect (structural, electronic and magnetic) which coexist at T_{M-I}.

Before proceeding to a more detailed presentation of the physical properties of $RNiO_3$ perovskites, we would like to recall an important feature of these oxides, namely, their perfect oxygen stoichiometry. In contrast to the high-T_c superconductors, where the non-stoichiometry is the basic tool to change the physical properties, $RNiO_3$ perovskites transform from metals to insulators, or from paramagnets to antiferromagnets, just by changing the temperature. Thus, all the difficulties associated with the description of the local disorder, which constitute one of the major problems found by the theoreticians trying to give a proper description of the ground state of the high-T_c superconductors, are absent from the nickelates.

Finally, it is important to stress that the basic feature which makes this system an almost ideal 'text-book example, is the *continuous* and *monotonic* dependence of the physical properties upon the size of the rare earth. This fact provides a remarkable opportunity to verify (or even to establish) several empirical relations, as well as to test some theoretical results concerning magnetism and M–I transitions.

In the following text, we present a summary of the experimental work made on this system during the last 6 years, as well as some (not yet published) recent high-pressure and very low-temperature results. The structural, magnetic and electronic properties will be successively reviewed, with an effort in each section to relate the results to those of the previous ones. In conclusion, a phase diagram relating structural changes and physical properties will be proposed.

2. Synthesis

As pointed out in the introduction, the $RNiO_3$ compounds were prepared for the first time by Demazeau *et al* in 1971 [1]; they succeeded in synthesizing the whole series of nickelates except those containing Ce, Pr and Tb (probably due to the intermediate III/IV oxidation state of these rare earth ions). Surprisingly, no studies (except for the first member of the series, $LaNiO_3$) have been published since this date up to 1989 [9]. The reason for this apparent lack of interest was in fact the extreme experimental conditions needed to carry out the synthesis procedure. Thus, whereas Ni(II) oxides are in general easily synthesized at low oxygen pressures ($\leqslant$1 bar) and high temperatures (800–1000 °C), the oxidation of Ni to Ni(III), necessary to obtain $RNiO_3$ perovskites, does not proceed in the former conditions, and either higher pressures or lower temperatures are necessary to stabilize the Ni^{3+} ion.

In their original work, the Bordeaux group used a mixture of R_2O_3, NiO and $KClO_3$ in molar proportions 1:2:1.5. A few grams of this mixture, enclosed in a sealed platinum crucible, were introduced into a 'Belt'-type pressure generator equipped with a microfurnace, and heated at 950 °C at a pressure of 60 kbar. With this procedure, the thermal decomposition of the potassium chlorate produces *in situ* a very high oxygen pressure, which allows the stabilization of the 3+ oxidation state of Ni. This procedure has the advantage of being very fast, but unfortunately, the experimental set-up ('Belt' pressure device) is not easily available for most inorganic chemistry laboratories. Moreover, the small volume of powder obtained in every synthesis (a few cubic millimetres) made it rather tedious, especially if a large volume of sample was needed for further measurements.

Recently, alternative procedures have been described by different authors [9, 2]. The

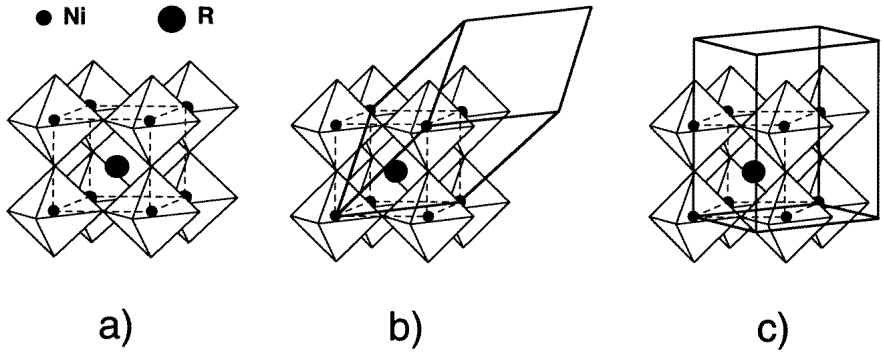

Figure 2. (a) The ideal perovskite structure (cubic $Pm\bar{3}m$). (b) Rhombohedral distortion ($R\bar{3}c$). (c) Ortho-rhombic distortion ($Pbnm$).

major interest of these new methods of synthesis is the fact that only moderate oxygen pressures and/or temperatures are needed. Thus, Vassiliou *et al* [9] succeeded in preparing $NdNiO_3$ at 650 °C in 1 bar oxygen, and Lacorre *et al* [2] were able to obtain $LaNiO_3$, $PrNiO_3$, $NdNiO_3$, $SmNiO_3$ and $EuNiO_3$ at 1000 °C and 150–200 bar. Other important advantages are (i) the better availability of the equipment, (ii) the possibility of producing larger amounts of sample and (iii) the availability of samples as sintered pellets, which is very convenient for performing transport measurements.

3. Crystallographic structure

3.1. Introduction

From the structural point of view, the $RNiO_3$ compounds are orthorhombically distorted perovskites [10]. The aristotype of this structural family, whose chemical formula can be written in a general way as ABX_3, is the mineral 'perovskite' ($CaTiO_3$). The ideal cubic structure, which is displayed by $CaTiO_3$ above 900 °C (see figure 2(a)), consists of a 3D array of corner-sharing BX_6 octahedra, located at the nodes of a simple cubic lattice. At the centre of the unit cell ((1/2 1/2 1/2) position) there is room for the A cation, which will fit perfectly if

$$d_{A-X} = d_{B-X}\sqrt{2}. \tag{1}$$

The stability of the perovskite structure requires X to be an anion and B a cation showing preference for octahedral coordination. The A position must be occupied by a cation with the adequate oxidation state (in order to assure the electrical neutrality) and whose size satisfies the condition (1). In the case of the $RNiO_3$ perovskites, the rare earth is too small to satisfy this criterion. Thus, the NiO_6 octahedra, which have been found to remain practically undistorted along the series, are tilted to fill the extra interstitial space. These rotations cause the unit cell to be smaller and more distorted than the ideal cubic cell. Since the magnitude of this distortion is related to the relative distances d_{Ni-O} and d_{R-O}, it can be discussed in terms of the tolerance factor [11] defined as

$$t = d_{A-X}/d_{B-X}\sqrt{2}. \tag{2}$$

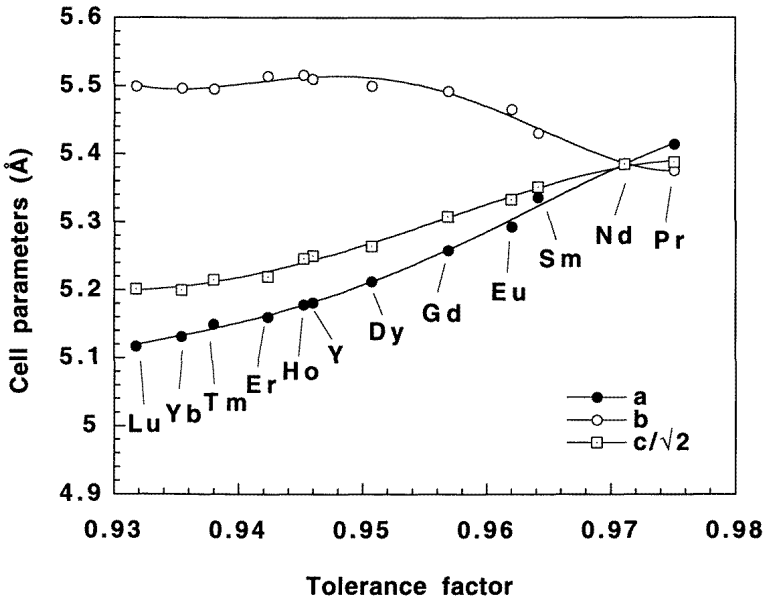

Figure 3. The variation of the lattice parameters as a function of the tolerance factor in the $RNiO_3$ series. The values of t have been calculated by using $d_{Ni-O} = 1.94$ Å (the same for all the nickelates) and the R–O distances given in [49] for trivalent rare earth ions in coordination 12.

Experimentally, it is observed that when t is slightly less than 1 unity, the NiO_6 octahedra are rotated around the [111] cubic axis [12] (figure 2(b)). For even smaller t, the octahedra tilt around the [110] and [001] cubic directions, resulting in the orthorhombic $GdFeO_3$ structure [13] (figure 2(c)). For $t < 0.7$ other, non-perovskite structures are preferred [10].

3.2. Room-temperature crystallographic structure

The earliest papers dealing with $LaNiO_3$, which were published four decades ago [14, 12], attributed to this compound the $R\bar{3}c$ rhombohedral symmetry (figure 2(b)). This assignment was confirmed in subsequent papers [1, 4]. The crystallographic structure of the remaining nickelates was, however, found to be orthorhombic and described by the space group $Pbnm$ ($GdFeO_3$ type, see table 1 and figure 2(c)).

In figure 3 we have represented the variation of the lattice parameters as a function of the tolerance factor. From this picture we deduce that the orthorhombic distortion, which becomes more important with decreasing radius of the rare earth ion, is stable from $t \approx 0.932$ (Lu) to $t \approx 0.975$ (Pr). In the case of $LaNiO_3$, the high value of the tolerance factor ($t \approx 0.986$) allows the less distorted rhombohedral structure to be stabilized. The boundary between these two phases has been situated by Lacorre *et al* at $t \approx 0.985$ [2].

An interesting trend, which has been observed in all the presently available nickelates (from $LaNiO_3$ to $EuNiO_3$) is the practical invariance of the average Ni–O distance (see table 1). The NiO_6 octahedra behave approximately as rigid bodies, the departure from the ideal perovskite structure along the series being due to their cooperative tilts. The cosine of

the tilt angle ω is, to a first approximation, a *linear* function of T_{M-I} [15]. Although this tendency has to be tested for the remaining nickelates, it strongly suggest that this angle is the relevant structural parameter controlling the evolution of T_{M-I} along the series.

3.3. The structural phase transition

Figure 1(b) shows the thermal evolution of the relative unit cell volume V/V_0 (V_0 is the volume at 1.5 K) for $PrNiO_3$, $NdNiO_3$ and $SmNiO_3$. These measurements clearly show the existence of a sudden (first-order), small expansion of the unit cell (about 0.2%) at the temperature where the M–I transition takes place.

The variation of the unit cell volume is the result of a small increase in the Ni–O distance (≈0.2%) and a simultaneous decrease of the Ni–O–Ni superexchange angle θ (≈0.4%, see figure 4). Here, θ is defined as $\theta \approx \pi\text{-}2\omega$, where ω is the tilt angle of the NiO_6 octahedra. The collective displacement of O atoms, shown schematically in figure 5, corresponds to coupled tilts of the octahedra in the sense of increasing rotation angles around the b and c axes. In other words, the structural changes simply consist of an enhancement of the orthorhombic distortion. Thus, within the experimental uncertainty imposed by the resolution, the crystallographic structure at $T < T_{M-I}$ is also well described in the $Pbnm$ space group.

A very interesting feature of this subtle structural transition is that the oxygen displacements seem to be merely a regular accommodation of the perovskite framework to the sudden enhancement of the Ni–O distance. This all happens as if a certain (probably electronic in origin) mechanism produces at $T = T_{M-I}$ a sudden increase of the Ni–O distance and then the structure reacts in a purely steric way by increasing the tilt angle of the octahedra. The magnitude and sign of the variation of the Ni–O–Ni angle θ can be easily derived by using the following expression [4]:

$$\Delta\theta_{Ni-O-Ni} \approx -275(d_{R-O}/d_{Ni-O}^2\sqrt{2})\,\Delta d_{Ni-O}. \tag{3}$$

The substitution of Δd_{Ni-O} by the observed value across the transition obtained from neutron diffraction measurements (≈ 0.0035 Å) yields $\Delta\theta_{Ni-O-Ni} \approx -0.46^\circ$. This is the expected $\Delta\theta$ value if steric effects predominate. Looking at figure 4, we see that it has the same sign and the same order of magnitude as the $\Delta\theta$ experimentally determined.

4. Transport properties

4.1. Electrical resistance

Perhaps the most interesting transport property in these compounds is their electrical resistance, whose temperature dependence for the first members of the series is shown in figure 1(a). As can be appreciated, $LaNiO_3$ remains metallic from 10 K to RT, whereas a very sharp M–I transition takes place for the remaining members of the series.

Although it is difficult to establish the nature of the gap only from resistance measurements, other valuable information can however be obtained. For example, in the case of $PrNiO_3$ and $NdNiO_3$, the low-temperature region can be reasonably well fitted by supposing a simple activated behaviour, the activation energies being respectively 22 and 25 meV [16, 17]. These activation energies are slightly larger than the thermal energy k_BT at $T = T_{M-I}$ (see table 2) but smaller than the gap estimated by optical measurements (between 100 and 250 meV for $NdNiO_3$ [18]) or by high-resolution ultraviolet photoemission (≈200 meV [19]). In any case, it is worth noting that these values are between one and

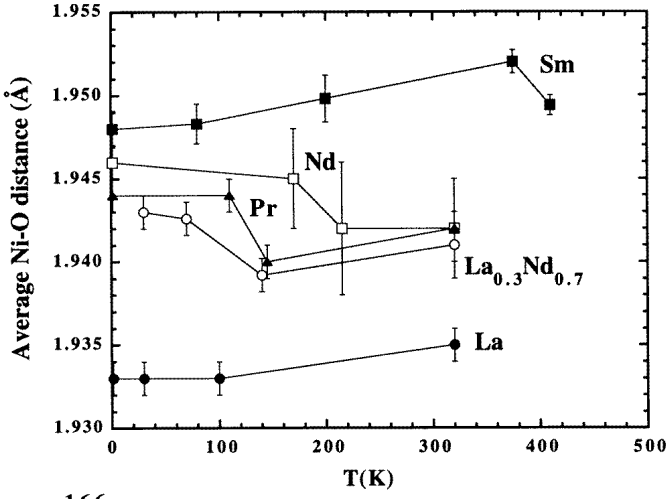

(a)

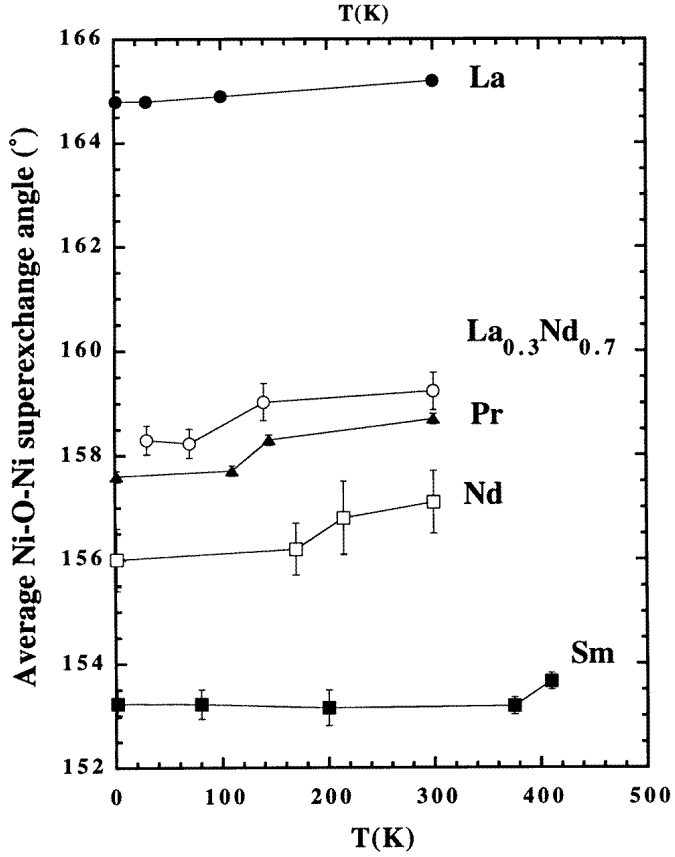

(b)

Figure 4. The thermal evolution of (a) the average Ni–O distance and (b) the average Ni–O–Ni angle for the nickelates with R = La, Pr, Nd [4], Sm [28] and $La_{0.3}Nd_{0.7}$ [22].

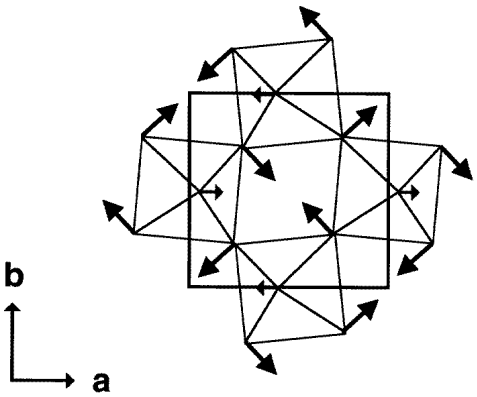

Figure 5. A scheme of the atomic displacements across the M–I transition (adapted from [4]).

Table 2. Thermal energies $k_B T_{M-I}$ for $RNiO_3$ perovskites.

	$k_B T_{M-I}$ (meV)
$LaNiO_3$	metallic
$PrNiO_3$	11.2
$NdNiO_3$	17.2
$SmNiO_3$	34.5
$EuNiO_3$	41.4

two orders of magnitude smaller than those reported for other Ni oxides ($E_g \approx 4$ eV in both NiO and La_2NiO_4 [20]).

4.2. The Seebeck coefficient

The nature of the carriers can be deduced from the sign of the Seebeck coefficient $S(T)$. Its thermal behaviour, which is displayed in figure 6(a) for $PrNiO_3$, shows a linear dependence for $T > T_{M-I}$. Moreover, it is small in magnitude and negative (≈ -10 μV K^{-1}). These values are typical for a metal with *e^--like particles as charge carriers*. Assuming a simple free-electron model, the observed slope of $S(T)$ in the metallic regime indicates an effective charge concentration of about 4.6×10^{20} e$^-$ cm^{-3}, that is, 0.025 e$^-$/Ni atom. If we compare this result with the effective electron densities of pure 3d transition metals (see for example [21]), we find a difference of about two orders of magnitude. $RNiO_3$ perovskites are, then, very bad metals. Even if this is only a very qualitative argument, this fact would explain the smallness of some of the effects (the structural changes (section 3) or the variation of the density of states (section 7)) observed at the M–I transition.

As expected across an M–I transition, $S(T)$ decreases abruptly below T_{M-I}, becoming very large in magnitude ($S = -270$ μV K^{-1} at 77 K). However, its sign is always negative, thus indicating that *carriers are also electrons in the insulating state*.

4.3. Hysteresis across the metal–insulator transition

Due to the first-order nature of the M–I transition, a coexistence of the high-temperature metallic phase and the low-temperature insulating phase over a certain temperature range

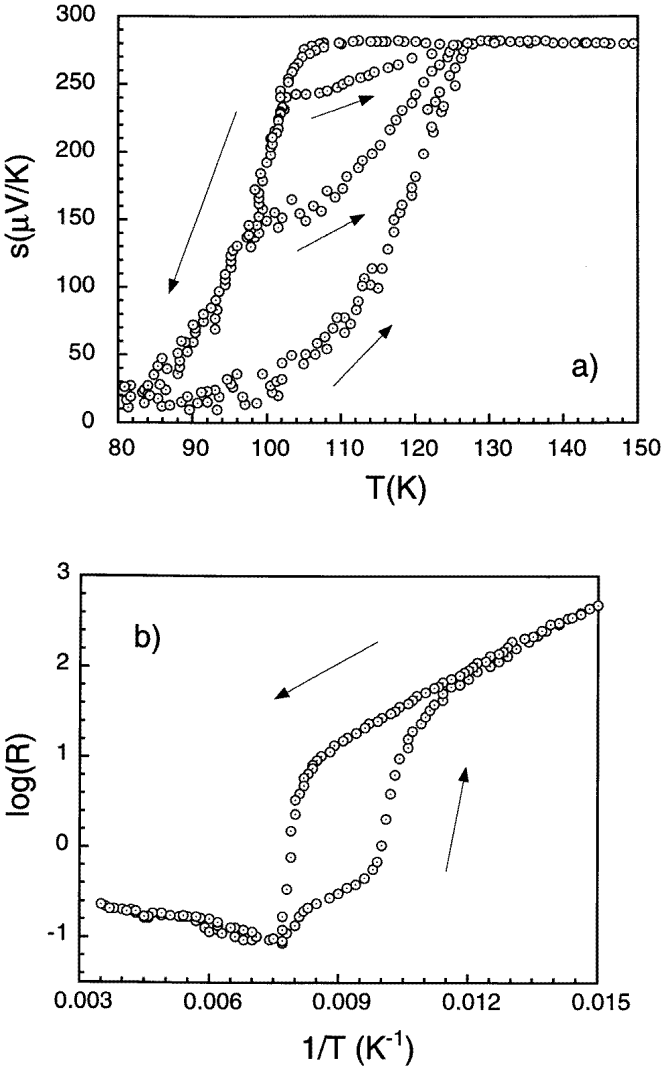

Figure 6. The hysteresis below $T_{M-I} = 130$ K in (a) the Seebeck coefficient and (b) the electrical resistance of $PrNiO_3$ (adapted from [16]).

close to T_{M-I} could be expected, thus leading to a hysteretic behaviour of the transport properties. Figure 6(a) shows the Seebeck coefficient and the resistance of $PrNiO_3$ measured in a cooling–heating cycle [16], where this hysteretic behaviour is clearly observed. Notice that the upper and lower limits of the hysteretic region (T_{M-I} and T_{CR}) *are well defined and do not depend, within the experimental resolution, on the thermal history of the sample*.

The analysis of these data has been performed by Granados *et al* [16], in terms of a mixture of metallic and semiconducting phases. They show that the temperature dependence of both the resistivity and the Seebeck coefficient can be well described by the expressions

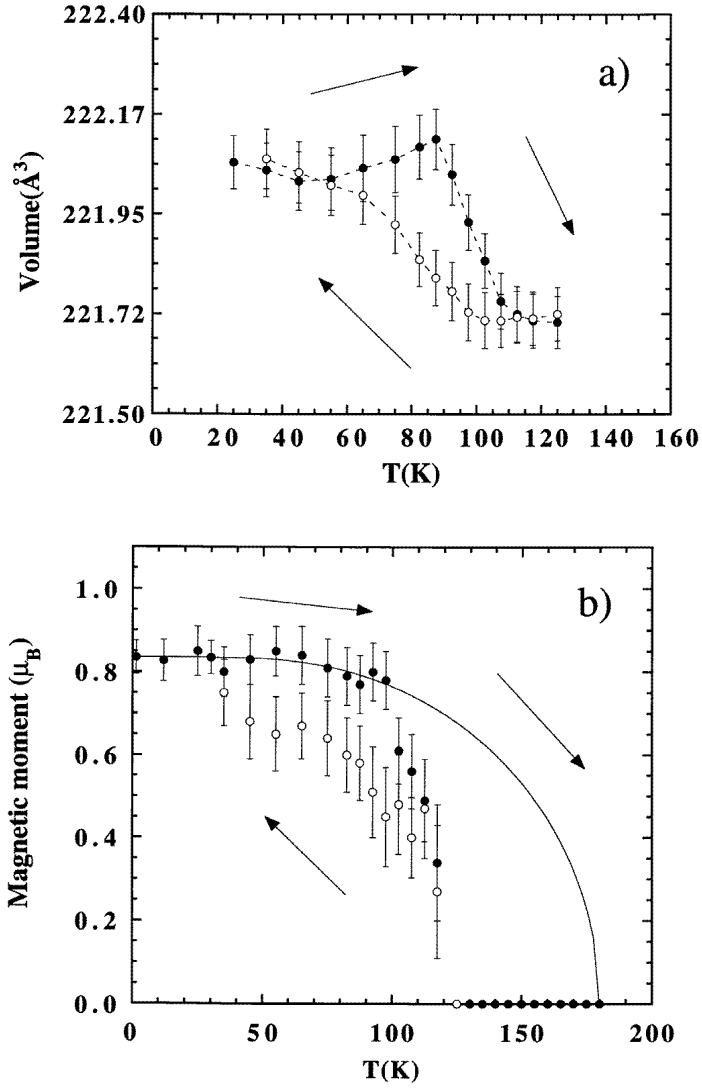

Figure 7. The hysteresis below $T_{M-I} = 104$ K in the unit cell volume and the Ni magnetic moment of $La_{0.3}Nd_{0.7}NiO_3$.

derived for transport properties of mixed systems and they have extracted the volume fraction of both the metallic and the insulating phase around $T_{M-I.}$ Their conclusions can be summarized as follows. Above T_{M-I}, only a metallic phase exists. Just below T_{M-I}, the semiconducting phase starts to nucleate, but the percolation of the metallic matrix continues down to lower temperatures. The suppression of the last connected path between metallic domains corresponds to the inflection point observed in the resistance at about 102 K. Finally, at T_{CR}, the transformation is accomplished, the sample becoming single phase and insulating for $T < T_{CR}$.

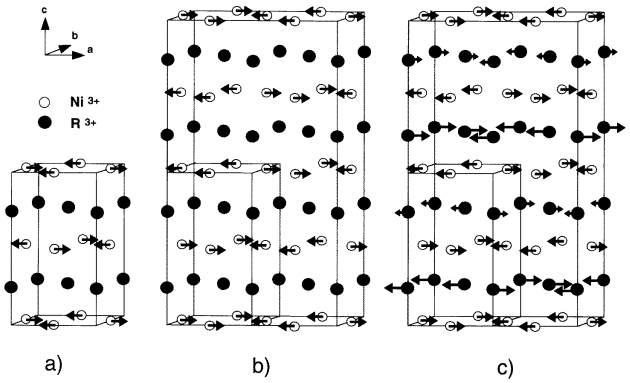

Figure 8. The magnetic structure of $PrNiO_3$: (a) as predicted by Demazeau *et al* [1] (notice that the absolute direction of the Ni magnetic moments has been arbitrarily chosen in this picture); (b) as found experimentally [27]. (c) The magnetic structure of $NdNiO_3$ [34] and $SmNiO_3$ [28] below 30 K.

The hysteretic behaviour has also been recently observed in the solid solution $La_{0.3}Nd_{0.7}NiO_3$ ($T_{M-I} \approx 104$ K) by means of neutron diffraction [22]. Figure 7 shows the evolution of the cell volume and the Ni magnetic moment (see section 5) around the M–I transition. Even if the accuracy of these data is lower than in the case of the transport measurements, the different rate of transformation on cooling and on heating is also clearly observable. Moreover, the evolution of the Ni sublattice magnetization on cooling indicates that *the ordered magnetic moments are only present in the insulating phase*.

5. Magnetic properties

5.1. Introduction

Before the nineties, very little was known about the magnetic behaviour of $RNiO_3$ compounds. For $LaNiO_3$, which was at that time the only available member of the series, some susceptibility measurements [23] as well as neutron diffraction studies [24] were however available. In these works, no evidence of magnetic ordering was found above 10 K, and the value and temperature dependence of the magnetic susceptibility were consistent with a Pauli paramagnetic behaviour.

Even though they synthesized 12 different rare earth nickelates, Demazeau and co-workers [1] reported magnetic susceptibility measurements only for $LaNiO_3$, $YNiO_3$ and $LuNiO_3$, that is, only for those compounds with diamagnetic R^{3+} ions. Thus, whereas their results for $LaNiO_3$ agree with those of Goodenough and Raccah [23], they found Curie–Weiss behaviour for $YNiO_3$ and $LuNiO_3$. A sudden increase of χ^{-1} at 145 K (Y) and 130 K (Lu) was interpreted as the onset of cooperative ordering of the Ni magnetic moments. From the refined values of the Curie constant they concluded that Ni ions were trivalent with the low-spin $t_{2g}^6 e_g^1$ configuration. The magnetic structure proposed by these authors is shown in figure 8(a) (G-type).

Since 1989, several authors reported magnetic susceptibility measurements on $PrNiO_3$ and $NdNiO_3$ [9, 25, 26]. Due to the enormous contribution of the Pr^{3+} and Nd^{3+} ions, no information could be derived about the behaviour of the Ni magnetic moments from

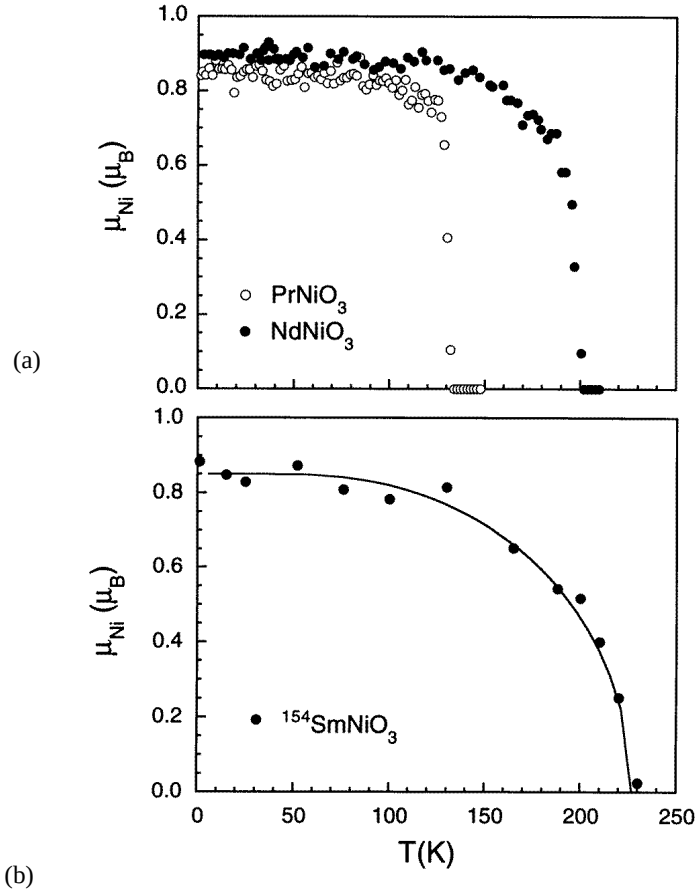

Figure 9. The thermal evolution of the Ni magnetic moment for different nickelates: (a) $PrNiO_3$ ($T_{M-I} = 130$ K) [33] and $NdNiO_3$ ($T_{M-I} = 200$ K) [27]; (b) $SmNiO_3$ ($T_{M-I} = 400$ K) [28].

their data. Concerning the remaining nickelates, no susceptibility measurements have been published so far, but the sudden decrease of the paramagnetic fraction observed by Torrance *et al* [3] in a muon spin rotation experiment (see figure 1(c)) suggests the onset of 3D magnetic ordering at $T_N = 130$ K (Pr), 200 K (Nd), 225 K (Sm) and 205 K (Eu). These results have been confirmed by recent neutron diffraction experiments in the cases of $PrNiO_3$, $NdNiO_3$ [27] and $SmNiO_3$ [28].

5.2. Magnetic structure

5.2.1. The Ni sublattice. The magnetic structure of $PrNiO_3$ and $NdNiO_3$ was solved by García-Muñoz *et al* [27], who observed the appearance of several small reflections below T_{M-I}. Their magnetic origin was probed by means of polarized neutrons and they were indexed with the propagation vector $\boldsymbol{k} = (1/2, 0, 1/2)$ ($\boldsymbol{k} = (1/4, 1/4, 1/4)$ in the pseudocubic parent perovskite cell). A similar magnetic structure has been recently found for $SmNiO_3$ [28].

The proposed magnetic structure (Ni sublattice) is shown in figure 8(b). The most interesting (and surprising!) feature of such a magnetic arrangement is that it supposes the existence of an equal number of ferromagnetic (F) and antiferromagnetic (AF) couplings between nearest neighbours. In other words, each Ni magnetic moment is coupled with three of its six nearest neighbours via an AF interaction (full lines), whereas the coupling with the three others is F (dotted lines). As far as we know, this magnetic arrangement is unprecedented in an oxide with perovskite structure.

Figure 9(a) shows the evolution of the ordered moments in the Ni sublattices of $PrNiO_3$ and $NdNiO_3$ down to 1.5 K. In the first compound, the Ni moments are completely saturated to approximately 1 μ_B (Ni^{III} low spin) just below T_N ($T_N = 135$ K), suggesting that the virtual Néel temperature is actually higher. In $NdNiO_3$ the situation is less clear, but the evolution of the Ni sublattice magnetization close to the M–I transition also suggests a virtual Néel temperature located somewhere in the temperature range between 210 and 250 K. This is confirmed by the well known positive correlation between T_N and the Ni–O–Ni superexchange angle θ [29]. As shown in figure 10, this angle decreases going from La to Lu†. Thus, extrapolating the experimentally observed T_N versus $\cos^2(\theta)$ dependence, we would expect the Néel temperature to be 257 K for $PrNiO_3$ and 250 K for $NdNiO_3$. As mentioned in the introduction, these two nickelates are the only ones where the electronic localization and the Néel state occur at the same temperature. Thus, the sudden disappearance of the 3D ordered magnetic moment can be directly related to the abrupt change from insulating to metallic conductivity. For the nickelates with $T_N < T_{M-I}$ (from Sm to Lu) the Néel state is not perturbed by the appearance of the metallic state and the Ni sublattice magnetization as a function of T displays a normal Brillouin-type dependence (see figure 9(b)).

5.2.2. The origin of the magnetic structure. In the orthorhombic *Pbnm* structure, the e_g orbitals are split into two non-degenerate $a_{g,1}$ and $a_{g,2}$ orbitals. Because of the orthorhombic distortion of the NiO_6 octahedra is very small, these orbitals can be expressed, at least to a first approximation, as a linear combination of the octahedral e_g orbitals $d_{x^2-y^2}$ and $d_{3z^2-r^2}$:

$$a_{g,1} = \alpha_1 d_{x^2-y^2} + \beta_1 d_{3z^2-r^2} \tag{4a}$$

$$a_{g,2} = \alpha_2 d_{x^2-y^2} + \beta_2 d_{3z^2-r^2}. \tag{4b}$$

If only one of the a_g orbitals were occupied, the Goodenough–Kanamori rules would predict the existence of AF coupling between the Ni magnetic moments. The expected magnetic structure is shown in figure 8(a). The experimentally observed arrangement in $PrNiO_3$, $NdNiO_3$ and $SmNiO_3$ is, however, very different (figure 8(b)), and it is in contradiction to a uniform occupation of the a_g orbitals (only one of them occupied).

A possible explanation has been proposed by García-Muñoz et al [28] following the theoretical calculations of Cyrot and Lyon-Caen [30]. These authors suggest that *the actually observed magnetic structure results from the occurrence of an orbital superlattice*. As the difference in energy between the $a_{g,1}$ and $a_{g,2}$ orbitals may be very small (perhaps not very different from the intra-atomic ferromagnetic exchange), the competition between intraatomic exchange correlations and the energy gain by the electrons occupying the lower-energy orbital can lead to a ground state in which the lattice breaks up into two sublattices,

† The value of the Ni–O–Ni superexchange angle θ is experimentally known for $LaNiO_3$, $PrNiO_3$, $NdNiO_3$ and $SmNiO_3$. For the remaining nickelates, only the lattice parameters are available [1]. However, by supposing that the NiO_6 octahedra are perfectly regular and behave as rigid bodies along the series, θ can be calculated as $\theta = \pi - 2a\cos(a^2\sqrt{2}/bc)$.

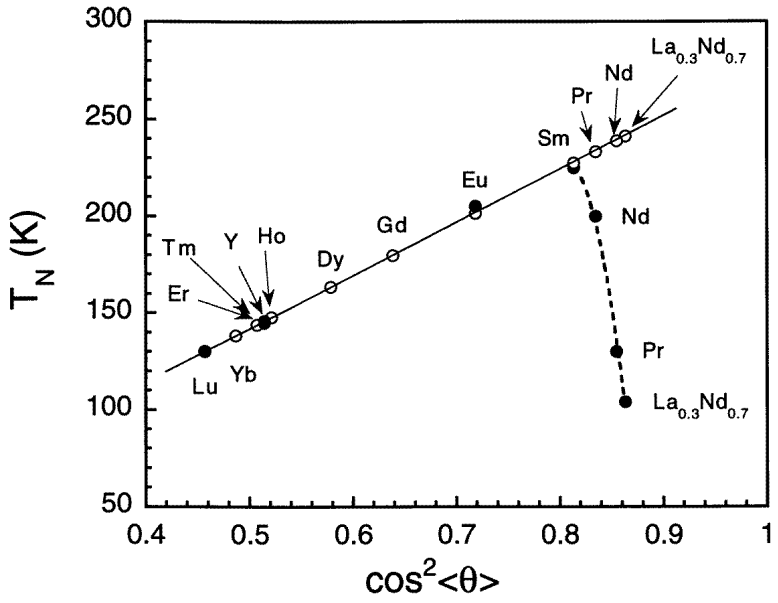

Figure 10. The evolution of T_N as a function of the average superexchange angle for the $RNiO_3$ series. The full dots correspond to the experimentally measured values and the open dots to the extrapolated values.

each with predominantly one of the $a_{g,1}$ or the $a_{g,2}$ orbitals half occupied. The nearest-neighbouring Ni atoms with the electron in the same orbital will be then AF coupled and those with a different orbital occupancies will prefer to align their $S = 1/2$ spins parallel. This situation is schematically shown in figure 11(a).

Another mechanism which may induce an orbital ordering is the the cooperative Jahn–Teller effect. This is for example the case in $LaMnO_3$ [31]. In this compound, the electronic configuration of Mn^{3+} is $t_{2g}^3 e_g^1$. To break the degenerancy of the e_g^1 orbitals, a strong elongation of the MnO_6 octahedra takes place. Thus, the $3d_{3z^2-r^2}$ orbital has lower energy than the $3d_{x^2-y^2}$ and the e_g^1 electron will be exclusively located in it†. The resulting orbital ordering is schematically shown in figure 11(b). In this case, the orientation of the e_g orbitals can be directly deduced from the alternating arrangement of the elongated MnO_6 octahedra. In $RNiO_3$ perovskites, however, *no appreciable Jahn–Teller distortion has been observed, the existence of an orbital superlattice being invoked uniquely to explain the existence of such an unusual magnetic structure.*

If the orbital ordering produces a significative distortion of the NiO_6 octahedra, it could be possible to observe superstructure peaks corresponding to the propagation vector $\boldsymbol{k} = (1/2\,0\,1/2)$ below T_{M-I}. In the case of $PrNiO_3$ and $NdNiO_3$, this is a difficult task due to the existence of magnetic reflections at exactly the same positions. $SmNiO_3$ is in principle a more suitable candidate because the magnetic and the M–I transitions are well separated.

† This description is again a first approximation to the problem. As in $RNiO_3$ perovskites, the NiO_6 octahedra present an orthorhombic distortion, the description in terms of $3d_{x^2-y^2}$ and $3d_{3z^2-r^2}$ being no longer valid. However, the use of the proper notation does not change the final conclusion, namely, the appearance of the orbital ordering displayed in figure 11(b).

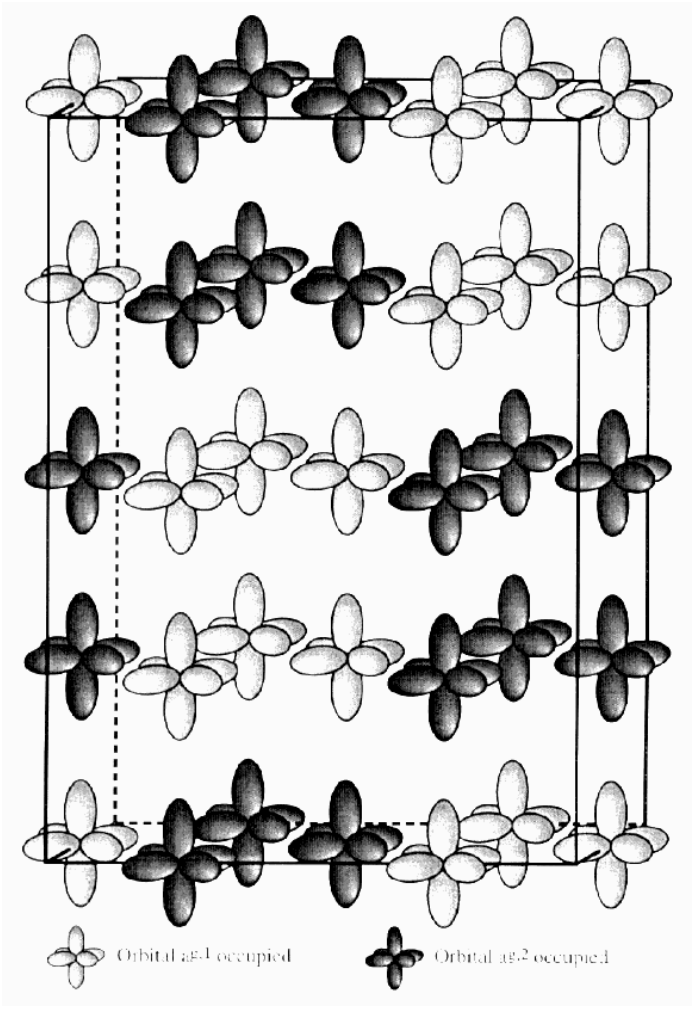

(a)

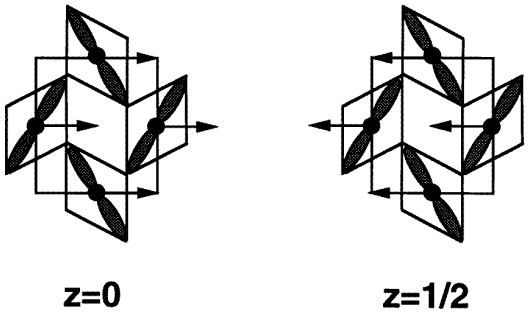

(b)

Figure 11. A schematic representation of the orbital superlattice (a) in $PrNiO_3$, $NdNiO_3$ and $SmNiO_3$ and (b) in $LaMnO_3$.

However, a recent high-intensity neutron powder diffraction experiment performed on a $^{154}SmNiO_3$ sample† indicates that, if they exist, the superstructure reflections are at least 10^4 times smaller than the largest nuclear reflection. The effective existence of the orbital ordering remains then to be demonstrated in $RNiO_3$ perovskites. Another possibility is that our ideas about superexchange interactions are too simplistic and the Goodenough–Kanamori rules do not apply to the present system. In any case, the existence of other subtle interactions able to stabilize the observed spin arrangement should not be disregarded.

5.2.3. The rare earth sublattice. Whereas in $PrNiO_3$ no traces of cooperative magnetic ordering have been found in the Pr sublattice, the sharp rise of some magnetic reflections observed below approximately 30 K indicate the existence of induced magnetic ordering of the Nd^{3+} moments in $NdNiO_3$. At $T \approx 200$ mK, a new, even sharper increase has been also observed [32, 33].

The proposed magnetic structure between 30 K and 200 mK [32–34] is shown in figure 8(c). Notice that, because of the particular arrangement of the Ni magnetic moments, the exchange field at the Nd positions is practically zero in half of them ($z = 3/8$, $7/8$) and different from zero in the other half ($z = 1/8$, $5/8$). The consequence is the existence of two different values for the Nd^{3+} magnetic moments (large and small arrows at the Nd positions in figure 8(c)) which at $T = 200$ mK are 2.0(2) μ_B ('large' Nd) and approximately 0.8(2) μ_B ('small' Nd).

Below 200 mK, two different hypotheses can be considered. As a first possibility, the diffraction patterns can be analysed by considering a 'normal' electronic magnetic origin for the extra intensity. In fact, it has been recently shown that it can be perfectly reproduced if the magnetic structure is basically the same as at 1.5 K, but with a sudden increase of the Nd magnetic moment taking place at approximately 200 mK (maybe the set-up of the Nd–Nd interactions). With this model, the refined magnetic moments at 10 mK are 2.8 and 0.7 μ_B. This possibility is, however, in contradiction with the magnetic ground state of Nd derived from crystal-field measurements. As shown in [33], the expected saturation moment of the Nd^{3+} ion in $NdNiO_3$ is approximately 2 μ_B, as the refined value just before the sudden increase of the magnetic reflections.

As a second possibility, the existence of a polarization of the Nd nuclear spins in the hyperfine field created by the electronic Nd magnetic moments may also be considered. The coherent signal from this effect is expected to be quite small since the abundance of the only two Nd isotopes with non-zero nuclear spin (^{143}Nd and ^{145}Nd) is only about 20% . However, recent investigations in other Nd-based perovskite compounds show that the contribution of the large nuclear moment of both isotopes ($I = 7/2$) as well as their unusually large incoherent Fermi lengths ($b_i = 21.1$ and 13 fm, respectively) are able to overcome this limitation [35]. The analysis of the neutron diffraction patterns by including this possibility gives a value of 2.1 μ_B for the 'large' Nd and a nuclear polarization along the [100] direction of 56(5)% [33].

6. High-pressure measurements

The first measurements of the electrical resistance under high pressures ($P_{max} \approx 15$ kbar) have been simultaneously reported by two independent groups [36, 37]. In both papers, the authors find a strong decrease of T_{M-I} with pressure (see figure 12). However, whereas

† The high neutron absorption cross section of the ^{149}Sm isotope prevents the realization of such an experiment using natural Sm.

Obradors *et al* [36] report a linear dependence of T_{M-I} on pressure, the data of Canfield and co-workers [37] fit better with an approximately quadratic function. The average values of $\partial T_{M-I}/\partial P$ reported by these authors are -4.2 K kbar^{-1} and -7.6 K kbar^{-1}, respectively, for pressures between 0 and 15 kbar. However, in both publications, $\partial T_{M-I}/\partial P$ appears to be *the same* for all the examined nickelates.

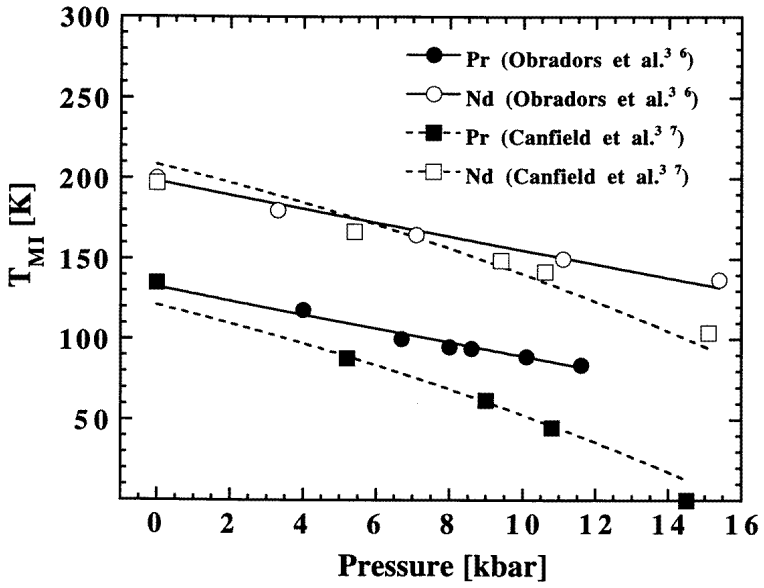

Figure 12. The pressure dependence of T_{M-I} ([36, 37]).

This last feature indicates that a common structural and/or electronic parameter is controlling the evolution of T_{M-I} with pressure. In the opinion of both Canfield and Obradors, this parameters is, as in the case of the internal pressure (substitution of one rare earth by another with a larger ionic radius), the Ni–O–Ni superexchange angle θ. However, *they predict respectively a positive and a negative sign for* $\partial\theta/\partial P$.

The first neutron diffraction experiments performed at relatively low pressures on $PrNiO_3$ (up to approximately 5 kbar) [38] indicated that the main structural changes consist of a small diminution of the Ni–O distance d_{Ni-O} and the simultaneous increase of the Ni–O–Ni superexchange angle θ (see figure 13). The sign of $\partial\theta/\partial P$ is then positive, as predicted by Canfield *et al*. Recent neutron powder diffraction experiments up to 80 kbar have fully confirmed the low-pressure results. Moreover, they have shown *that, for pressures higher than approximately 40 kbar, the symmetry of the unit cell changes from orthorhombic (Pbnm) to rhombohedral* ($R\bar{3}c$) [39, 40]. The evolution of the structure under external pressure is then qualitatively similar to that observed by substituting the rare earth ion by another with larger ionic radius (chemical pressure). In both cases a less distorted perovskite framework, together with enhanced metallic conductivity, is progressively reached. A detailed quantitative study of the differences between these two mechanisms is currently in progress.

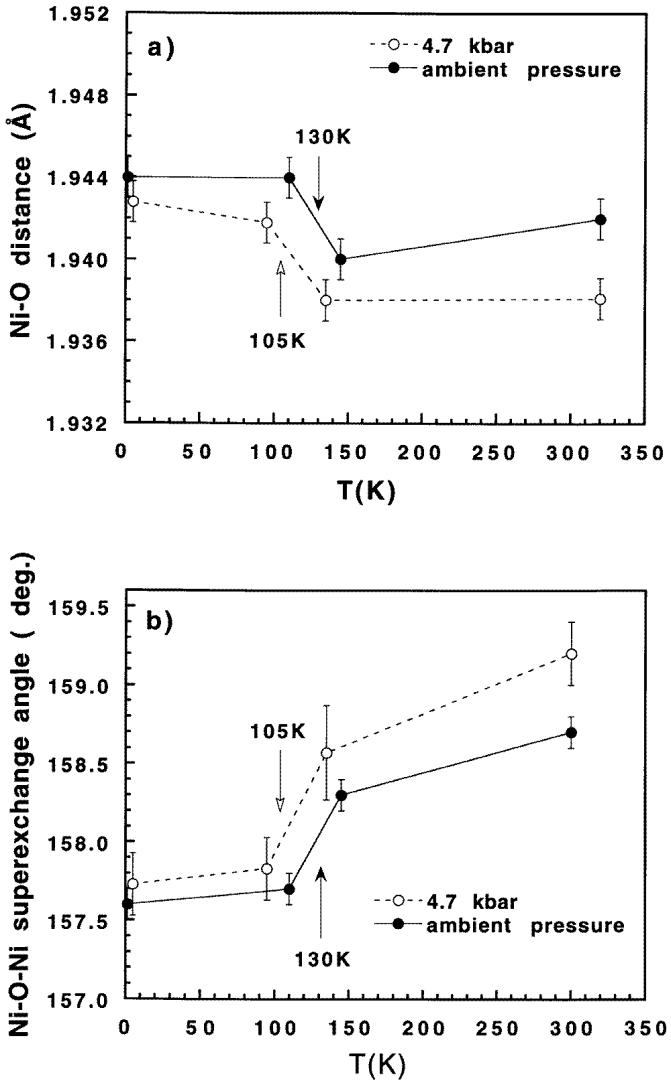

Figure 13. The pressure dependences of the average Ni–O distance and the average Ni–O–Ni angle in $PrNiO_3$ [38].

7. Electronic structure

7.1. Introduction

In section 1, it was pointed out that the $RNiO_3$ perovskites are one of the few families of oxides to show metallic conductivity. Why these compounds are metals and most of the transition metal (TM) monoxides (MnO, FeO, CoO, NiO, CuO), TM perovskites $LaTMO_3$ (TM = V, Cr, Mn, Fe, Co) or La_2TMO_4 (K_2NiF_4-like) compounds (TM=Co, Ni, Cu) are insulators has been for 40 years an open question. From elementary electron band

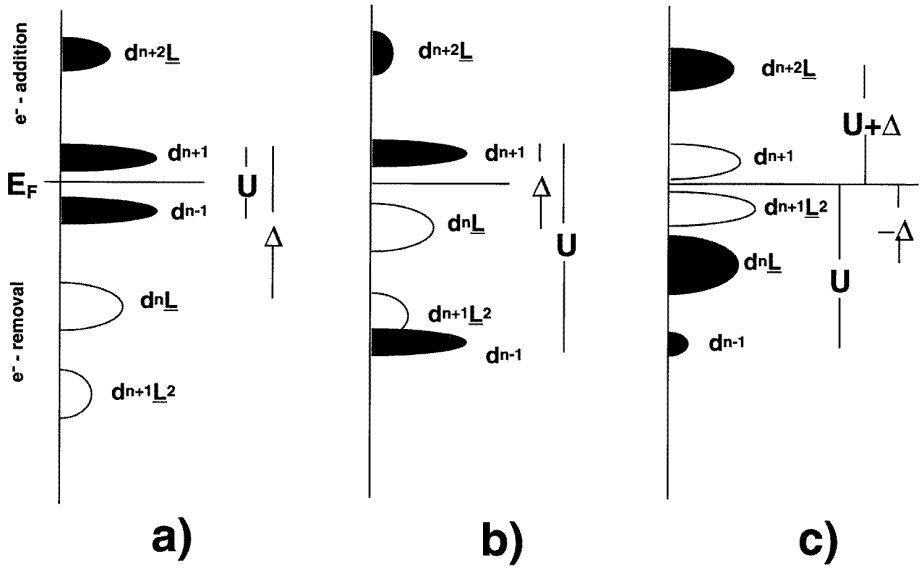

Figure 14. A schematic representation of the single-particle density of states (DOS) for the (a) Mott–Hubbard, (b) charge-transfer and (c) negative-Δ insulators. The shaded and open areas represent respectively the TM 3d- and ligand O 2p-derived DOS.

structure calculations, which can be considered as the simplest approach to the problem, compounds in which the TM cation has an odd number of electrons are expected to be metallic, whereas those with an even number of electrons would be insulating. However, these predictions are not verified by most of the TM oxides (see, for example, the excellent review by Torrance *et al* [8]). Although more sophisticated band structure calculations can be used to examine each compound in detail, the use of this approach for the description of the electronic structure of TM oxides has been and is still seriously controversial. The main reason is the difficulty in properly taking into account the effects of (i) the electronic correlation (very important for the late TMs) and (ii) the appearance of magnetic ordering, which have been shown to be crucial features in an understanding the electronic behaviour of these compounds.

An alternative, very simple and rather powerful method has been developed by Zaanen *et al* [41]. The most interesting feature of this approach is that, using only a few parameters (fundamental electronic energies), it has been able to account for the electronic behaviour of a great number of 3d TM oxides. The parameters involved are (i) the d–d Coulomb interaction U (which also includes exchange), defined as the excitation energy necessary to produce charge fluctuations of the type $d_i^n d_j^n \Rightarrow d_i^{n-1} d_j^{n+1}$ (here i and j label 3d metal sites and n the 3d orbital occupation), (ii) the charge-transfer energy Δ, defined as $E(d_i^{n+1} d_j^n \underline{L}) - E(d_i^n d_j^n)$, where $\underline{L}$ represents an anion (ligand) hole, and (iii) the ligand (W) and metal (w) one-electron bandwidths (see figure 14). Thus, by comparing the corresponding values of U, Δ, W and w, TM oxides can be easily classified as insulators (Mott–Hubbard if $W < U < \Delta$ and charge transfer if $W < \Delta < U$) or metals (low U if $U < w$ and low Δ if $\Delta < W$).

Since the predictions of this formalism depend (not only!) on correct values of U, Δ,

W and w, it would be interesting to have a simple method to estimate them. A very nice procedure has been recently developed by Torrance *et al* [8] who, using only crystallographic data, gas-phase ionization potentials and Madelung energies, have been able to reproduce the electronic behaviour of a great number of oxides.

The prediction of these authors for $RNiO_3$ perovskites places these compounds not in the metallic but in the insulating region, although very close to the dividing line between charge-transfer insulators and low-Δ metals. Thus, *within the framework of this simple model, the M–I transition would take place due to the opening of a charge-transfer type gap below* T_{M-I}. This mechanism is schematically shown in figure 15. The narrowing of the O 2p-derived valence band is caused by the less efficient overlap of the Ni 3d and O 2p orbitals in the insulating phase.

In spite of the support given to the charge-transfer model by the discovery of the M–I transition in the nickelates with R $\neq$ La, there is a debate concerning the mechanism responsible for the electronic localization in these compounds [5]. Thus, recently, Mizokawa *et al* [42] pointed out that, with increasing atomic number or increasing formal valence of the metal element, Δ systematically decreases. These authors stressed that Δ may become very small or negative with unusually high valences such as Fe^{4+}, Ni^{3+} or Cu^{3+}. In this case, the $d^{n+1}\underline{L}$ configuration should be as favourable as or even more favourable than the $3d^n$ one. The expected charge fluctuations in the metallic state are of the type $d^{n+1}\underline{L}d^{n+1}\underline{L} \Rightarrow d^{n+1}d^{n+1}\underline{L}^2$ and the existence of a gap would be only possible in the presence of O 2p–O 2p hole correlations strong enough to split the O 2p band (p–p gap; see figure 14). This seems to be the case for the insulator $NaCuO_2$, where XPS measurements and the cluster calculation reported by Mizokawa *et al* [42] give a value of $\Delta = -2(\pm 1)$ eV. Following these authors, the gap in $NaCuO_2$ is neither of the Mott–Hubbard type nor of the charge-transfer type, but of the p–p type.

Like Cu in $NaCuO_2$, Ni in $RNiO_3$ shows an unusually high (3+) formal valence. However, the existence of a p–p gap in the insulating state would require a $3d^8\underline{L}$ (Ni^{2+} O^-) ground-state configuration instead of the classical assumption $3d^72p^6$ (Ni^{3+} O^{2-}). Even if the valence-bond calculations indicate that the latter possibility is a good starting point for an understanding of the electronic structure of these compounds [4], the absence of Ni^{3+} reported for systems as $Ni_{1-x}Li_xO$ or $La_{2-x}Sr_xNi_{4+\delta}$ raises severe doubts about the validity of such a crude description.

From the analysis of the x-ray absorption and photoemission spectra, a more realistic ground state, which includes the Ni–O hybridization, has been recently proposed. Thus, the relevant electronic structure of this nickelates can be described as a mixture of the $3d^72p^6$ (Ni^{3+} O^{2-}) and the $3d^8\underline{L}$ (Ni^{2+} O^-) configurations. In the next sections we will discuss the experimental facts which lead to this conclusion and the degree of mixing proposed by the different authors as well as its relevance in deciding between the different mechanisms responsible for the M–I transition.

7.2. Spectroscopic measurements

7.2.1. X-ray absorption.

O 1s edge. Figure 16 shows the O 1s edges of $LaNiO_3$, $PrNiO_3$ and $NdNiO_3$ measured at RT [5]. The most important feature is the sharp and intense pre-peak situated at 528.4 (La), 528.6 (Pr) and 528.8 (Nd) eV, whose integrated intensity decreases when going from La to Pr (9%) and Nd (20%). A similar structure is also present in the NiO O 1s edge (see figure 17), but its position (532 eV) is about 3 eV higher than that of the $RNiO_3$ pre-peak. This feature, which has been also found in the O 1s edges of the other TM monoxides, is

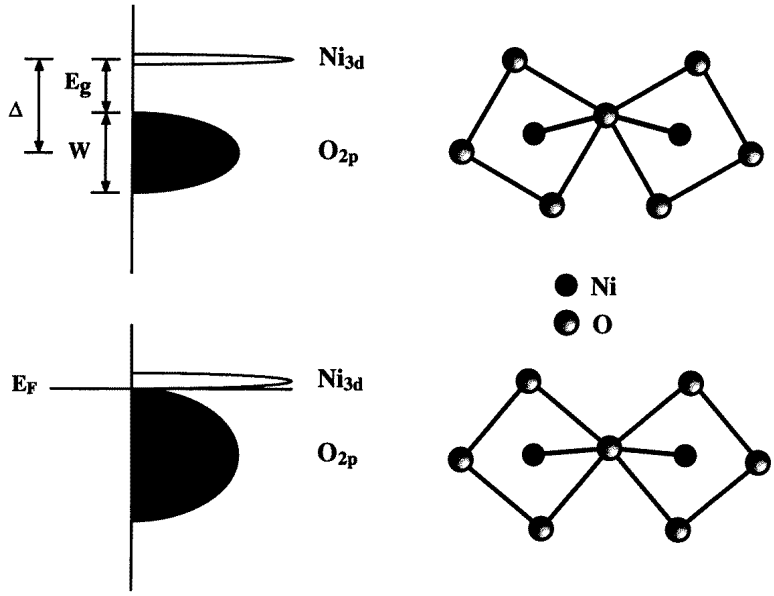

Figure 15. The M–I transition in the charge-transfer scheme. The narrowing of the O 2p-derived valence band below T_{M-I} would take place because of the less efficient overlap of the O 2p and Ni 3d orbitals produced by the decrease of the Ni–O–Ni superexchange angle.

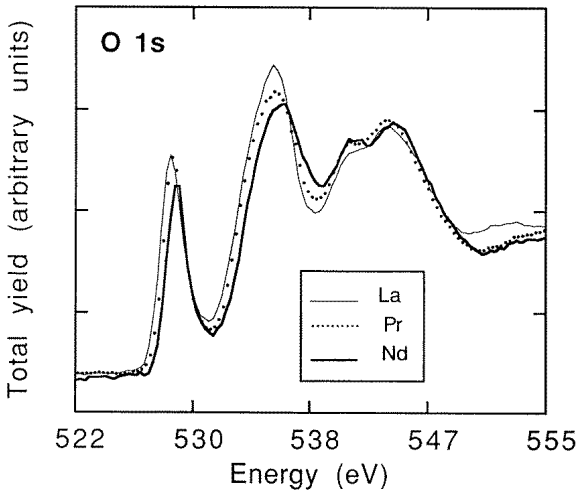

Figure 16. O 1s edges of $LaNiO_3$, $PrNiO_3$ and $NdNiO_3$ at RT [5].

due to the O 2p weight in states of predominantly Ni 3d character.

To explain the origin of the sharp pre-peak structure, it is necessary to introduce the Ni 3d and O 2p hybridization. Though very different methods have been used in the literature to describe covalency effects, the most widely used among XAS spectroscopists

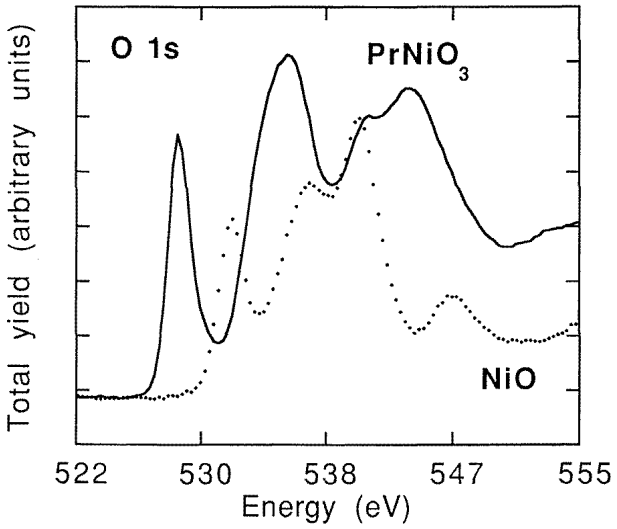

Figure 17. O 1s edges of $PrNiO_3$ and NiO at RT [5].

is the configuration interaction method. Within this formalism, the partial charge transfer from the anion to the cation is described by adding to the original ionic configuration an admixture of configurations in which one or more electrons have been transferred. In the $RNiO_3$ case, we can write the ground state of an 'ionic' NiO_6 octahedral cluster as

$$|\Psi^G_{ionic}\rangle = |3d^7 2p^6\rangle \tag{5}$$

and including covalency as

$$|\Psi^G_{covalent}\rangle = \alpha|3d^7 2p^6\rangle + \beta|3d^8\underline{L}\rangle + \gamma|3d^9\underline{L}^2\rangle. \tag{6}$$

Here, $\alpha^2 + \beta^2 + \gamma^2 = 1$ and usually $\gamma \ll \beta < \alpha$. The values of α, β and γ can in principle be obtained by combining the results of several x-ray spectroscopies. At the O 1s K edge, and allowing only intra-atomic XAS transition matrix elements, the intensity of the pre-peak is proportional to β^2 and it is a measure of the covalency in the ground state. Thus, it should be very useful to compare the integrated intensities of the NiO (see figure 17) and the $RNiO_3$ pre-peaks since, for the first compound, several calculations of the degree of hybridization are available. Unfortunately, the presence of R 4f and 5d orbitals prevents a direct comparison since is impossible to perform a correct normalization.

Although it is hard to quantify the values of α and β without performing a full configuration-interaction calculation, they can be estimated by using the well known dependence of the Ni 3d–O 2p transfer integrals, T_{pd}, on the interatomic distance ($T_{pd} \sim \beta \sim 1/d^{3.5}_{Ni-O}$) [43]. In NiO, Ni atoms are surrounded by six equivalent O atoms ($d_{Ni-O} = 2.090$ Å) and the ground state can be described as $|\Psi^G_{covalent}\rangle = \alpha|3d^8 2p^6\rangle + \beta|3d^9\underline{L}\rangle + \gamma|3d^{10}\underline{L}^2\rangle$ with $\alpha^2 \approx 0.82$, $\beta^2 \approx 0.18$ and $\gamma^2 \approx 0$ [44]. In the $RNiO_3$ compounds, $\langle d_{Ni-O}\rangle = 1.942$ Å. Thus, using the $T_{pd} \sim \beta \sim 1/d^{3.5}_{Ni-O}$ dependence, we find a value of $\beta^2(RNiO_3) = 0.30$ for the weight of the $3d^8\underline{L}$ configuration. Though it is only approximate, *this result suggests that the Ni 3d–O 2p hybridization is stronger in $RNiO_3$ than in NiO*.

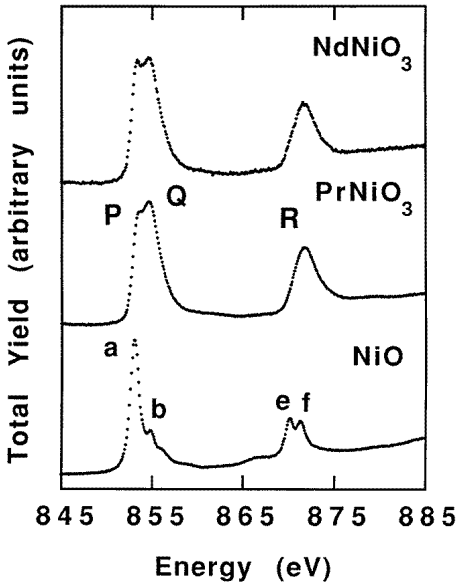

Figure 18. Ni 2p edges of NiO, $PrNiO_3$ and $NdNiO_3$ at RT [5].

Ni 2p edge. In figure 18 the RT Ni 2p edges for the compounds $PrNiO_3$, $NdNiO_3$ and NiO are shown [5]. Ni 2p edges of divalent Ni compounds, as NiO or Ni dihalides, have been extensively studied during recent years. The main features appearing in the spectra are quite similar in all the divalent compounds, and the presence of small satellites or the decrease of the multiplet splitting with smaller anion electronegativities is now well understood in terms of a covalent ground state of mainly Ni^{2+} ($3d^8$) character plus an anion-dependent fraction of the $3d^9\underline{L}$ and $3d^{10}\underline{L}^2$ configurations.

For Ni^{3+} compounds, both experimental results and theoretical calculations are quite scarce. To our knowledge, the only published Ni 2p edges on compounds containing nominally trivalent Ni ions are those of $PrNiO_3$ and $NdNiO_3$ [5, 7], and the only available theoretical calculations of the Ni^{3+} 2p XAS edge have been performed by de Groot *et al* [45], considering a pure $3d^7$ configuration. Intuitively, the Ni^{3+} 2p edge will show a much richer multiplet structure and higher integrated intensity than Ni^{2+} due to its extra 3d hole. The experimental data, which show much broader structures than NiO, can in principle be interpreted as corresponding to Ni^{3+}. Unfortunately, the absence of fine structure does not allow a direct comparison with the available calculations [45]. It should be noted that, in this case, broadening is not due to the lack of experimental resolution. The quality of the NiO spectrum, obtained with the same experimental set-up, is comparable with the data obtained with the Dragon monochromator [46, 47] thus indicating that the origin of the broadening is an intrinsic property of the sample.

In order to obtain additional information about the Ni 3d–O 2p hybridization, it is very interesting to compare the $RNiO_3$ spectra with the much more accessible Co^{2+} octahedrically coordinated experimental data [45]. Due to the atomic origin of the main features appearing in the 2p absorption edges of 3d transition metals, we expect strong similarities between Co^{2+} and Ni^{3+} spectra due to their common $3d^7$ configuration. Thus, looking at the data

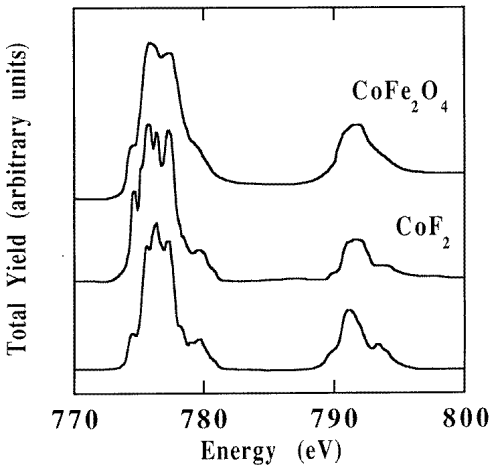

Figure 19. Co 2p edges of $CoFe_2O_4$ and CoF_2. Bottom, a theoretical calculation of the Co 2p edge [5].

reported by Sette *et al* [46, 47] (see figure 19) for the Co 2p edge of the inverse spinel $CoFe_2O_4[CoFe]\{Fe\}O_4$, we found very similar structures, which gives us confidence in the validity of our hypothesis. A possible origin for the small differences between the two spectra is the different spin state of Co^{2+} (high spin in $CoFe_2O_4$) and Ni^{3+} (low spin in $RNiO_3$). Calculations including high- and low-spin states are necessary in order to establish their influence on the XAS spectra.

It is also very interesting to compare the Co 2p edges of $CoFe_2O_4$ and CoF_2 (rutile-type structure). In both compounds Co^{2+} shows octahedral coordination and high-spin configuration ($t_{2g}^5 e_g^2$), but important differences between Co–O and Co–F bonds are expected due to the stronger electronegativity of the fluorine ion. Thus, covalency is expected to be more important in the oxide that in the fluoride. Looking at the spectra, the similarities between the Co 2p edges of the two compounds are evident. However, the fine structure predicted by the atomic theoretical calculations is clearly visible only in the latter. Taking into account the more ionic nature of the Co–F bonding, we can tentatively establish a direct correlation between spectral smearing and covalency. Although this is only a very qualitative argument, it explains the smooth shape of the $RNiO_3$ spectra and gives additional support to the existence of a highly hybridized ground state in these compounds.

Ni 1s edge. An extensive experimental and theoretical analysis of the Ni K edge on $LaNiO_3$ and $NdNiO_3$ has been performed by García *et al* [6]. By using the multiple-scattering formalism, they were able to extract the degree of mixing of the Ni 3d and O 2p orbitals in the ground state. The proposed weights of the $3d^7 2p^6$ and $3d^8\underline{L}$ configurations were 60 and 40%, respectively. This result agrees qualitatively with that derived from the analysis of the O 1s edge (70 and 30%), the degree of mixing being even larger.

7.2.2. Photoemission. X-ray and ultraviolet photoemission experiments have been reported by different authors [7, 48]. An interesting point revealed by these measurements is that the analysis of the spectra using configuration-interaction calculations seems to give support to the charge-transfer scheme ($\Delta \approx 1$–2 eV). The valence band, which for a charge-transfer

insulator is expected to be mainly of O 2p parentage, has however been shown to be Ni 3d based, at least in the vicinity of the Fermi level (down to −1.5 eV). This finding has been used to explain the evolution of the XPS spectra across the M–I transition reported in [19]. The loss of spectral weight on going from the metallic to the insulating state would correspond to a reduction of Ni 3d character in the valence band, as expected from the structural changes observed across the transition.

Another interesting, but rather surprising conclusion, is that the degree of hybridization of the Ni 3d and O 2p orbitals derived from these measurements is much larger than that reported in previous works. Mizokawa *et al* [7], for example, found a ground state constituted by 24% of $3d^7 2p^6$ and 76% $3d^8\underline{L}$. The weight of the $3d^8\underline{L}$ configuration would be much more important than that of the $3d^7$ one. The situation in the nickelates seems however to be different from that encountered in $NaCuO_2$. As previously mentioned, the refined value of Δ is small but positive, in contrast with the negative value (−2 eV) reported for $NaCuO_2$. The charge transfer model for the transition seems then to be more reliable than the opening of a p–p gap, but a clear experimental verification is still lacking.

8. Summary and conclusions

In the foregoing text, the structural, magnetic and electronic behaviour of $RNiO_3$ perovskites has been presented. As mentioned in section 1, a close connection exists between the physical properties and the steric effects associated with the decrease in size of the lanthanide ions. The relevant parameter controlling the metal–insulator temperature T_{M-I}, and the Néel temperature T_N as well as the stability of the different crystallographic structures found along the series is the Ni–O–Ni superexchange angle θ. The increasing overlap between the O 2p and Ni 3d orbitals which occurs on moving from Lu ($r_a = 0.977$ Å) to La ($r_a = 1.160$ Å) favours the metallic state (T_{M-I} decreases) as well as the AF state (T_N increases). The collapse of both tendencies occurs for $r_a \approx 1.10$ Å, T_N being identical to T_{M-I} for the nickelates with larger ionic radius ($NdNiO_3$ and $PrNiO_3$). This behaviour is illustrated in figure 20, where the evolution of T_{M-I}, T_N and the orthorhombic–rhombohedral transition temperature T_{R-O} as a function of r_a has been displayed.

The results of the different techniques reviewed along the paper give some elements for the understanding of the mechanism responsible for the M–I transition in the nickelates. The most important points to be retained are the following.

(i) The change in the transport properties at T_{M-I} is abrupt.

(ii) The associated structural changes are also discontinuous although very small.

(iii) A rather unusual 3D antiferromagnetic order develops in the insulating state, which, within the framework of the current theories about superexchange in oxides, can be only explained by supposing the existence of an orbital superlattice.

The three kinds of effect (structural, electronic and magnetic) which coexist at T_{M-I} (at least for $PrNiO_3$ and $NdNiO_3$), suggest several possibilities for the driving mechanism of the gap opening. A magnetic origin, which was at the beginning one of the most exiting possibilities, has been recently disregarded after the observation in $SmNiO_3$ ($T_N \neq T_{M-I}$) of the same magnetic structure as in the nickelates with $T_{M-I} = T_N$. To definitively reject this possibility, it would be however necessary to verify whether, as in the case of high-T_c superconductors, magnetic correlations are still present in the $T_N < T < T_{M-I}$ range.

Concerning the possibility of a Jahn–Teller distortion, high-intensity neutron diffraction experiments show that, if they exist, the superstructure peaks associated with the orbital

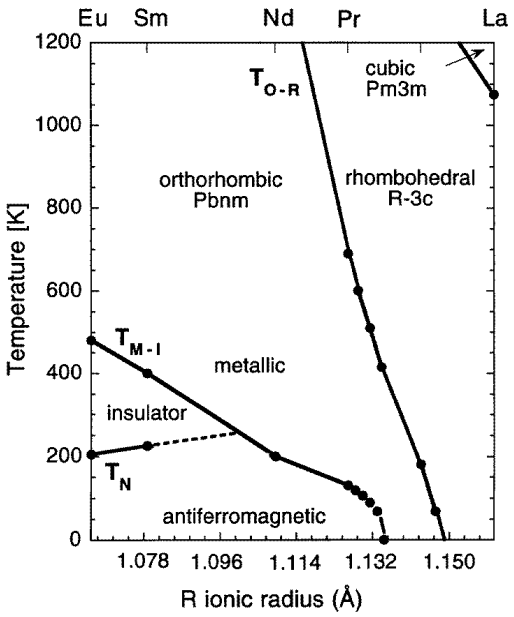

Figure 20. Phase diagram for the $RNiO_3$ perovskites.

ordering are at least 10^4 times smaller than the main nuclear peaks. Thus, within the present experimental accuracy, the structural changes below T_{M-I} simply consist of an enhancement of the orthorhombic distortion existing at higher temperatures. Single crystals and/or high-intensity synchrotron measurements would be necessary to decide about the existence of an additional structural distortion concomitant with the M–I transition.

Considering pure (not magnetic) electronic correlation, three kinds of gap are likely to occur: Mott–Hubbard type, charge-transfer type and negative-Δ type. The first estimation of Δ and U reported by Torrance *et al* [8] for $LaNiO_3$ gave $U - \Delta \approx 5$ eV, that is, they suggested the opening of a charge transfer gap below T_{M-I}. The experimental verification of the hypothesis, which has since remained the consensus view, is however not straightforward. Though some x-ray spectroscopic measurements are actually available, their analysis is far from trivial and depends strongly on the particular technique used.

In summary, the nature of the mechanism responsible for the M–I transition in $RNiO_3$ perovskites is still an open question. Though some 'key' experiments (most of them rather difficult to realize) would help to decide between the different possibilities, one of the major limitations to advance in our current understanding is the limited scope of the actual theories. More sophisticated mechanisms going beyond the classical ideas about superexchange in oxides should be considered, as well as new models and/or interactions able to produce M–I transitions.

Acknowledgments

I would like to thank S W Lovesey for his interest in this work. Helpful and stimulating discussions with A Fontaine, J L García-Muñoz, M Grioni, P Lacorre, R Lémanski, M W

Long, J Mesot, J Rodríguez-Carvajal and S Rosenkranz, as well as the critical reading of the manuscript by P Fischer and A Furrer, are also gratefully acknowledged. This work has been supported by the CEE under grant No ERB4001GT921221.

References

[1] Demazeau G, Marbeuf A, Pouchard M and Hagenmuller P 1971 *J. Solid State Chem.* **3** 582
[2] Lacorre P, Torrance J B, Pannetier J, Nazzal A I, Wang P W and Huang T C 1991 *J. Solid State Chem.* **91** 225
[3] Torrance J B, Lacorre P, Nazzal A I, Ansaldo E J and Niedermayer C 1992 *Phys. Rev.* B **45** 8209
[4] García-Muñoz J L, Rodríguez-Carvajal J, Lacorre P and Torrance J B 1992 *Phys. Rev.* B **46** 4414
[5] Medarde M, Fontaine A, García-Muñoz J L, Rodríguez-Carvajal J, de Santis M, Sacchi M, Rossi G and Lacorre P 1992 *Phys. Rev.* B **46** 14 975
[6] García J, Blasco J and Proietti M G 1995 *Phys. Rev.* B **52** 15 823
[7] Mizokawa T, Fujimori A, Arima T, Tokura Y, Mori N and Akimitsu J 1995 *Phys. Rev.* B **52** 13 865
[8] Torrance J B, Lacorre P, Asavaroengchai C and Metzger R 1991 *J. Solid State Chem.* **90** 168
[9] Vassiliou J, Hornbostel M, Ziebarth R and Disalvo F J 1989 *J. Solid State Chem.* **81** 208
[10] *Landolt–Börnstein, New Series* 1970 Group III, vol 4a, ed K H Hellwege and A M Hellwege (Berlin: Springer) ch 3, p 126.
[11] Goldschmith V M 1926 *Skr. Nor. Vidensk. Akad. Mat. Naturvidensk. Kl.* **2** 1
[12] Wold A, Post B and Banks E 1957 *J. Am. Chem. Soc.* **79** 4911
[13] Geller S 1956 *J. Chem. Phys.* **24** 1236
[14] Bertaut E and Forrat F 1956 *J. Physique Radium* **17** 129
[15] Medarde M, Rosenkranz S and Lacorre P in preparation
[16] Granados X, Fontcuberta J, Obradors X and Torrance J B 1992 *Phys. Rev.* B **46** 15 683
[17] Granados X, Fontcuberta J, Obradors X, Mañosa J L and Torrance J B 1993 *Phys. Rev.* B **48** 11 666
[18] Katsufuji T, Okimoto Y, Arima T and Yokura Y 1995 *Phys. Rev.* B **51** 4830
[19] Medarde M, Purdie D, Grioni M, Hengsberger M, Baer Y and Lacorre P 1997 *Europhys. Lett.* submitted
[20] Eisaki H, Uchida S, Mizokawa T, Namatame H, Fujimori A, van Elp J , Kuiper P, Sawatzky G A, Hosoya S and Katayama-Yoshida H 1992 *Phys. Rev.* B **45** 12 513
[21] Ashcroft N W and Mermin N D 1988 *Solid State Physics* (Tokyo: Holt-Saunders) ch 1, p 5
[22] Medarde M, García-Muñoz J L, Rosenkranz S, Lacorre P and Fischer P 1994 *Physica* B **194–196** 367
[23] Goodenough J B and Raccah P 1965 *J. Appl. Phys.* **36** 1031
[24] Koehler W C and Wollan E O 1957 *J Phys. Chem. Solids* **2** 100
[25] Xu X Q, Peng J L, Li Z Y, Ju H L and Greene R L 1993 *Phys. Rev.* B **48** 1112
[26] Blasco J and García J 1994 *J. Phys.: Condens. Matter* **6** 10 759
[27] García-Muñoz J L, Rodríguez-Carvajal J and Lacorre P 1992 *Europhys. Lett.* **20** 241
[28] Rodríguez-Carvajal J, Rosenkranz S, Medarde M, Lacorre P and Trounov V 1997 *Phys. Rev.* B submitted
[29] Goodenough J B 1963 *Magnetism and the Chemical Bond* (New York: Wiley)
[30] Cyrot M and Lyon-Caen C 1975 *J. Physique* **36** 253
[31] Quezel-Ambrunaz S 1968 *Bull. Soc. Fr. Mineral. Cristallogr.* **91** 339
[32] Rosenkranz S 1992 *LNS-Report* 165, Zürich
[33] Rosenkranz S 1996 *PhD Thesis* ETH Zürich 11 853
[34] García-Muñoz J L, Rodríguez-Carvajal J and Lacorre P 1994 *Phys. Rev.* B **50** 978
[35] Marti W, Medarde M, Rosenkranz S, Fischer P and Furrer A 1995 *Phys. Rev.* B **52** 4275
[36] Obradors X, Paulius L M, Maple M B, Torrance J B, Nazzal A I, Fontcuberta J and Granados X 1993 *Phys. Rev.* B **47** 12 353
[37] Canfield P C, Thompson J D, Cheong S W and Rupp L W 1993 *Phys. Rev.* B **47** 12 357
[38] Medarde M, Mesot J, Lacorre P, Rosenkranz S, Fischer P and Gobrecht K 1995 *Phys. Rev.* B **52** 9248
[39] Medarde M, Mesot J, Rosenkranz S, Lacorre P, Marshall W, Klotz S, Loveday J S, Hamel G, Hull S and Radaelli P 1997 *Physica* B **235–237**
[40] Medarde M, Mesot J, Rosenkranz S, Marshall W, Hull S and Lacorre P *Phys. Rev. Lett.* submitted
[41] Zaanen J, Sawatzky G A and Allen J W 1985 *Phys. Rev. Lett.* **55** 418
[42] Mizokawa T, Namatame H, Fujimori A, Akeyam K, Kondoh H, Kuroda H and Kosugi N 1991 *Phys. Rev. Lett.* **67** 1638
[43] Harrison W A 1980 *The Electronic Structure and Properties of Solids* Freeman, San Francisco
[44] Elp J van 1991 *PhD Thesis* University of Groningen

[45] de Groot F M F, Grioni M, Fuggle J C, Ghijsen J, Sawatzky G A and Petersen H 1989 *Phys. Rev.* B **40** 5715
[46] Sette F, Chen C T, Ma Y, Modesti S and Smith N V 1991 *X-Ray Absorption Fine Structure* ed F S Hafnain (London: Horwood)
[47] Sette F and Chen C T 1990 *Proc. 2nd Eur. Conf. on Progress in X-Ray Synchrotron Radiation Research* ed A Balerna, E Berrieri and S Mobilio (Bologna: SIF)
[48] Barman S R, Chainani A and Sarma D D 1994 *Phys. Rev.* B **49** 8475
[49] Poix P 1970 *C. R. Acad. Sci., Paris* **270** 1852